CONF-821155--4

INTERNATIONAL MEETING ON RESEARCH AND

TEST REACTOR CORE CONVERSIONS FROM

HEU TO LEU FUELS

CONF-821155--4

DE83 007725

Argonne National Laboratory

November 8-10, 1982

COMPARISON OF CALCULATED QUANTITIES WITH MEASURED QUANTITIES FOR THE LEU-FUELED FORD NUCLEAR REACTOR*

M. M. Bretscher and J. L. Snelgrove

RERTR Program

Argonne National Laboratory

*Work performed under the auspices of the U.S. Department of Energy

EHB

Comparison of Calculated Quantities with Measured Quantities for the LEU-Fueled Ford Nuclear Reactor

M. M. Bretscher and J. L. Snelgrove

Argonne National Laboratory

I. Introduction

The Ford Nuclear Reactor (FNR) went critical on December 8, 1981 with 23 LEU fuel elements. Five of these 23 elements were fabricated by CERCA and the others by NUKEM. Since that time a substantial data base of experimental results for LEU cores has been accumulated by the University of Michigan FNR staff. This paper compares some of the experimental data with analytical calculations based, for the most part, on three-dimensional diffusion theory. The critical configuration, control rod worths, axial rhodium reaction rate profiles and thermal flux distributions have been calculated and compared with measurements.

II. Critical Configuration

Figure 1 shows the FNR critical configuration with 23 fresh LEU fuel elements. The 18 plate standard FNR LEU fuel elements were fabricated by NUKEM and CERCA and contain about 167 g ^{235}U per element. Control elements contain 9 fuel plates. For this critical assembly the ^{235}U mass was 3512.82 g. With the shim safety rods (A, B and C) fully withdrawn and the control rod fully inserted, the excess reactivity was measured to be 0.067%. The worth of the hollow stainless steel control rod was found to be 0.383% so that the excess reactivity of the cold, clean LEU core was about 0.45%.

Five-group cross sections, based on the ENDF/B Version IV data base, were generated for each reactor region by the EPRI-CELL code (1). These multigroup cross section generation methods are described in the Guidebook (2). Table I shows the energy structure of the standard five-group set.

Using these cross sections, two- and three-dimensional diffusion calculations were performed to evaluate the eigenvalue for the 23-element, cold, clean LEU core. For these calculations all rods are withdrawn and each fuel element is represented by three regions -- a fuel region sandwiched between two side plate regions. Effects from the vertical H_2O-filled tubes which penetrate part way into the D_2O tank and from neutron leakage through the beam tubes have been ignored in these calculations. Table II summarizes the eigenvalues calculated from two-and three-dimensional models for both course and fine mesh structures. The XYZ fine mesh calculation gives an excess reactivity of 0.37%, somewhat less than the 0.45% measured value. Our experience with HEU cores has been to slightly overpredict the eigenvalue, but for this LEU core we have underpredicted k_{eff}.

III. Shim Safety Rod Worths

The FNR shim safety rods are made from borated stainless steel containing 1.5 w/o natural boron. Each of the solid rods has a 3.470 cm × 5.668 cm cross section with rounded ends having a radius of curvature of 1.099 cm. They are described in Ref. (3).

To calculate the rod worths, group-dependent internal boundary conditions (defined as current-to-flux ratios) were applied at the surface of the absorber in diffusion calculations. These boundary conditions were evaluated from P_1 S_8 transport theory calculations.

Cross sections for the outer, middle and inner regions of the rod were generated by the EPRI-CELL code in cylindrical geometry. Since the rod is essentially black to thermal neutrons, the outer radius of the cylindrical rod was chosen so as to preserve the surface area of the actual rod. The outer region of the rod was 1 mm thick and the middle layer 3 mm thick.

Current-to-flux ratios were evaluated in the P_1 S_8 approximation using both one-dimensional cylindrical and two-dimensional XY geometries. For each model the surface area of the shim safety rod was preserved and for the XY geometry the volume was also held constant. In both cases internal boundary conditions were evaluated at the surface of the borated steel rod. The ONEDANT (4) transport code was used for the one-dimensional problem and TWOTRAN-II (5) for the XY geometry. Average boundary conditions were obtained by perimeter weighting of the TWOTRAN point current-to-flux ratios. The results of these calculations are summarized in Table III. Because of modeling deficiencies, the ONEDANT internal boundary conditions tend to be too large and the TWOTRAN values somewhat small.

Control rod worths were measured in a 27-element and a 30-element LEU core. These two core configurations are illustrated in Figs. 2a and 2b. For each of the configurations the worths of the shim safety rods were evaluated in two dimensional XY calculations using the internal boundary conditions given in Table III. The results are summarized in Table IV where the calculated-to-experiment (C/E) worth ratios are shown for each of the shim safety rods. Doubling the number of mesh intervals in the core would increase these C/E ratios by about 2%. The shim rod worths are reasonably well-calculated for the 27-element core, but are underpredicted for the 30-element case.

A 3D model of the FNR reactor with 27 fresh LEU fuel elements has been used to calculate the differential worth of shim safety rod A. For these calculations each fuel element was again divided into two non-fuel regions, corresponding to the side plates, and a central fuel region. A 6 × 6 mesh structure in the XY plane was chosen for most fuel elements. For the control fuel elements, however, the mesh structure was 7 × 8. Axial mesh planes were separated by 2.50 cm in the core region except near the core-axial reflector interfaces where the spacing was reduced to 0.50 cm. The shim rods were represented as having a rectangular cross section whose dimensions were chosen so as to preserve the volume and surface area of the actual borated steel absorber. TWOTRAN internal boundary conditions (see Table III) were applied at the absorber surface.

For all these 3D calculations the control rod was assumed to be withdrawn half way. Shim rods B and C were moved as a unit in such a way as to keep the reactor near critical for each step of withdrawal of shim rod A. The DIF3D code (6), with internal boundary conditions, was used to calculate the eigenvalues corresponding to each withdrawal step and these results are summarized in Table V. The rod position for the fully inserted rod is taken as 0.0 inches (bottom of core) and 24.12 inches for the fully withdrawn rod. Figure 3 compares the calculations with the measured differential worth of shim rod A. Note that the 3D calculation gives a total rod worth which is about 4.5% larger than that found on the basis of the 2D - XY calculation.

IV. Axial Rhodium Reaction Rate Distributions

Axial reaction rate distributions were measured in the FNR with a rhodium self-powered neutron detector. Fig. 4 shows the core configuration of the 29 LEU fuel elements used during these measurements. A 3D model of this 29-element FNR reactor was used to calculate axial reaction rate distributions for the rhodium detector. For these calculations it was assumed that each of the shim rods was 20.7 inches withdrawn from the bottom of the core and that the control rod was withdrawn half way. Shim rods were treated using the same TWOTRAN internal boundary conditions as before (Table III). The fuel element mesh structure discussed earlier was again used in these DIF3D calculations of the XYZ fluxes from which the rhodium reaction rate traverses were determined. Reaction rate distributions calculated with and without equilibrium xenon and samarium were found to be nearly identical.

Measured and calculated axial rhodium capture rate distributions are compared in Figs. 5-11 for fuel element positions (FEP) 15, 19, 27, 35, 39, 47 and 37 (see Fig. 4). The curves are normalized at the peak of the distributions. In general, the measured and calculated distributions agree quite well, but in all cases the calculations underpredict the peak heights in the axial reflector regions. These calculated peak heights are very sensitive to the aluminum-water volume fractions used to describe the various axial reflectors. To illustrate this, Fig. 12 shows the axial capture rate distribution in fuel element position 37 (FEP37) where the aluminum end boxes above and below the fuel plates were explicitly represented in the 3D model. Comparing this figure with the previous one shows the improved agreement in the reflector peak regions.

The distribution in the H_2O reflector (grid position 40) is shown in Fig. 13. It is seen that the measured rhodium capture rate distribution in the light water reflector is broader and shifted with respect to the calculated one.

For measurements in the heavy water reflector, one inch diameter (I.D.) vertical tubes penetrate the D_2O tank to a depth of eight inches below the top of the core and are filled with H_2O. Fig. 14, taken from Ref. (7), shows these tubes entering the top of the D_2O tank and also identifies positions X, S, W and R. Rhodium capture rate distributions at locations X and S in the heavy water reflector are shown in Figs. 15 and 16. As Fig. 15 shows, the H_2O-filled tubes produce additional moderation in the D_2O tank, which is the reason for the discontinuity in the calculated capture rate distribution at the D_2O-H_2O interface at the bottom of tube X. This effect is not as evident at position S (Fig. 16) because this location is farther from the core. In the H_2O region above the D_2O tank the measured capture rate distribution, for some reason, does not fall off as rapidly as the calculated one.

V. Thermal Neutron Flux Distributions

The rhodium self-powered neutron detector (Ref. 7, pp.77 ff) was used to measure thermal neutron flux distributions in the 31-element LEU core. This core contains 25 standard fuel elements and 6 nine-plate control fuel elements. Using techniques already described, this core was modeled in XYZ geometry for diffusion calculations. For these calculations the control rod was withdrawn half way and the shim safety rods were banked at the 20.7 inch position. The H_2O-filled tubes at positions X, S, W and R in the D_2O tank (see Fig. 14) were explicitly represented in the 3D model. These tubes penetrate the heavy water tank to a depth of 8 inches below the top of the fuel.

Figure 17 shows the 31-element core configuration and the calculated-to-experiment (C/E) thermal flux ratios. The calculated thermal fluxes (group 5) were normalized to the measured value on the core midplane at grid position 37. In addition, measurements were made at the 1/4 and 3/4 core height positions so that the three numbers in a given grid location (Fig. 17) correspond to the C/E values at the lower, middle and upper elevations. In the 3D model these elevations correspond to axial positions for Z = 45, 60 and 75 cm. Because of access limitations, measurements in the D_2O tank were made only on the Z = 78.26 cm plane. The calculated axial flux distributions were used to extrapolate the measured values at positions X, W, S and R to the core midplane and the 3/4 height position. Measurements in the H_2O reflector were made at four locations in grid position 40 in order to define the thermal neutron flux peak in the reflector. The measurement at grid position 57 was in the central water hole of the 9 plate special fuel element. For most positions the C/E thermal flux ratios are within 10% of unity.

Figure 18 shows the calculated and measured thermal neutron flux distributions in row 7. Flux peaking in the water hole associated with the special fuel element at grid position 57 and in the H_2O reflector regions is clearly evident. Secondary peaks in the core correspond to the side plate regions containing Al-H_2O mixtures. In general, the agreement between the calculated and measured fluxes is quite good at both the middle and upper elevations.

Figure 19 shows a North/South traverse through the middle of column 3 and then is displaced 1.5 inches to the west at the core-D_2O tank interface so as to pass through positions X and S in the D_2O tank. Note the flux peaking in the upper elevation distribution in the H_2O-filled tube at position X (Y = 72.28 cm) in the D_2O tank. The effect is much less evident at position S. No such peaking is seen in the midplane distribution since the H_2O-filled tubes do not extend this deep into the D_2O tank. Figure 20 shows similar curves with the upper part of the traverses displaced in the opposite direction so as to pass through positions W and R in the D_2O reflector. In general, these distributions are in satisfactory agreement with the measured values.

In Figs. 17-20 the thermal fluxes are normalized to the experimental value on the midplane of position 37 and are in units of 10^{13} n/cm^2·s at a power of 2 MW. The 3D diffusion calculation was also done for a 2 MW power level, but the normalization required multiplying the calculated fluxes by a factor of 0.646. Thus, there is a large disagreement between the measured and calculated absolute fluxes (C/E = 1.55). This discrepancy remains to be resolved. The upper energy boundary of group 5 is 0.625 eV whereas the cadmium cutoff energy is about 0.55 eV. This difference accounts for some of the discrepancy.

ACKNOWLEDGEMENTS

The data upon which these comparisons are based was supplied by staff members from The University of Michigan Department of Nuclear Engineering. This cooperation is gratefully acknowledged.

References

1. B. A. Zolotar, et al., "EPRI-CELL Description," Advanced Recycle Methodology Program System Documentation, Part II, Chapter 5, Electric Power Research Institute (September 1977).

2. Research Reactor Core Conversion from the Use of Highly Enriched Uranium to the Use of Low Enriched Uranium Fuels Guidebook, pp. 448 ff, IAEA-TECDOC-233, (1980).

3. W. Kerr, et al., "Low Enrichment Fuel Evaluation and Analysis Program, Summary Report for the Period January 1980-December 1980," The University of Michigan Report (March 1981), Appendix C.

4. R. Douglas O'Dell, et al., "Users' Manual for ONEDANT: A Code Package for One-Dimensional, Diffusion-Accelerated, Neutral-Particle Transport," October 1980.

5. K. P. Lathrop and F. W. Brinkley, "TWOTRAN-II: An Interfaced, Exportable Version of the TWOTRAN Code for Two-Dimensional Transport," LA-4848-MS, July 1973.

6. D. R. Ferguson and K. L. Derstine, "Optimized Iteration Strategies and Data Management Considerations for Fast Reactor Finite Difference Diffusion Theory Codes," Nucl. Sci. Eng. 64, 593 (1977), and K. L. Derstine, ANL Internal Memoranda on the DIF3D Code (1977-1982).

7. W. Kerr, et al., "Low Enrichment Fuel Evaluation and Analysis Program, Summary Report for the Period January 1979 - December 1979," The University of Michigan Report (January 1980), Appendix B.

Table I. Energy Boundaries of Standard Five Group Structure

Group	Upper Energy Bound
1	10.0 MeV
2	0.8208 MeV
3	5.531 keV
4	1.855 eV
5	0.625 eV

Table II. Diffusion Theory Calculations for the FNR LEU Cold Clean Critical Configuration

Model	Mesh in Standard Fuel Element	k_{eff}
2D-XY	$N_x\ N_y = 6 \times 6$	1.00066
2D-XY	$N_x\ N_y = 10 \times 12$	1.00292
3D-XYZ	$N_x\ N_y = 6 \times 6$	1.00193
3D-XYZ	$N_x\ N_y = 10 \times 12$	1.00371
	Measured Value:	1.0045

Table III. Group-Dependent Internal Boundary Conditions ($-j/\phi$)

Group	E_u - eV	TWOTRAN-XY ($-j/\phi$)	ONEDANT-R ($-j/\phi$)
1	10.00 + 7	2.8411 - 2	3.5206 - 2
2	8.208 + 5	-8.3937 - 3	-1.2773 - 2
3	5.531 + 3	7.9673 - 2	1.0147 - 1
4	1.855	2.4479 - 1	2.7691 - 1
5	6.249 - 1	4.1490 - 1	4.4703 - 1

Table IV. Reactivity Worths of the FNR Shim Safety Rods

No. of Fuel Elements	Rod	Lattice Position	Exp. % $\Delta K/K$	C/E TWOTRAN-XY	C/E ONEDANT-R
27	A	46	2.220	0.989	1.051
27	B	48	2.320	0.974	1.035
27	C	26	2.283	0.947	1.006
30	A	46	2.742	0.955	1.015
30	B	48	2.313	0.910	0.968
30	C	26	2.166	0.881	0.937

Table V. Calculated FNR Shim Rod A Differential Worth in 27-Fuel-Element Core

Step	Rod A Position Inches	Rod B and C Position Inches	K-Effective	Δρ %	Total ρ %
1	24.12 (out)	13.04	1.002732	0.000	0.000
2	19.94	13.04	1.001214	0.151	0.151
3	16.00	13.04	0.997602	0.362	0.513
4	16.00	16.00	1.006252		
5	12.06	16.00	1.000362	0.585	1.098
6	8.12	16.00	0.993904	0.650	1.748
7	8.12	20.92	1.002876		
8	4.19	20.92	0.998774	0.410	2.158
9	0.00 (In)	20.92	0.997358	0.142	2.300

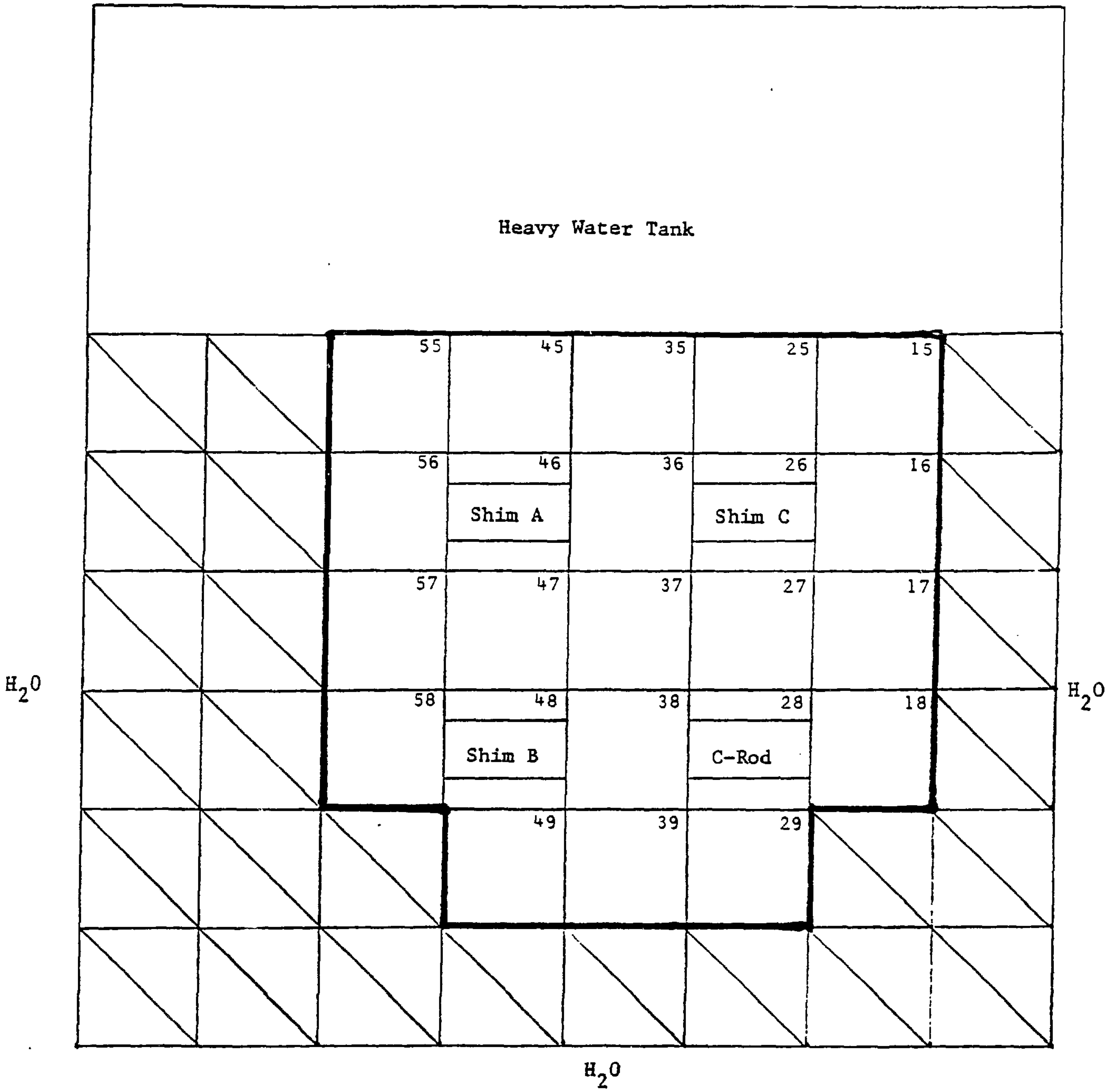

Fig. 1 FNR Initial LEU Critical Configuration (December 8, 1981)

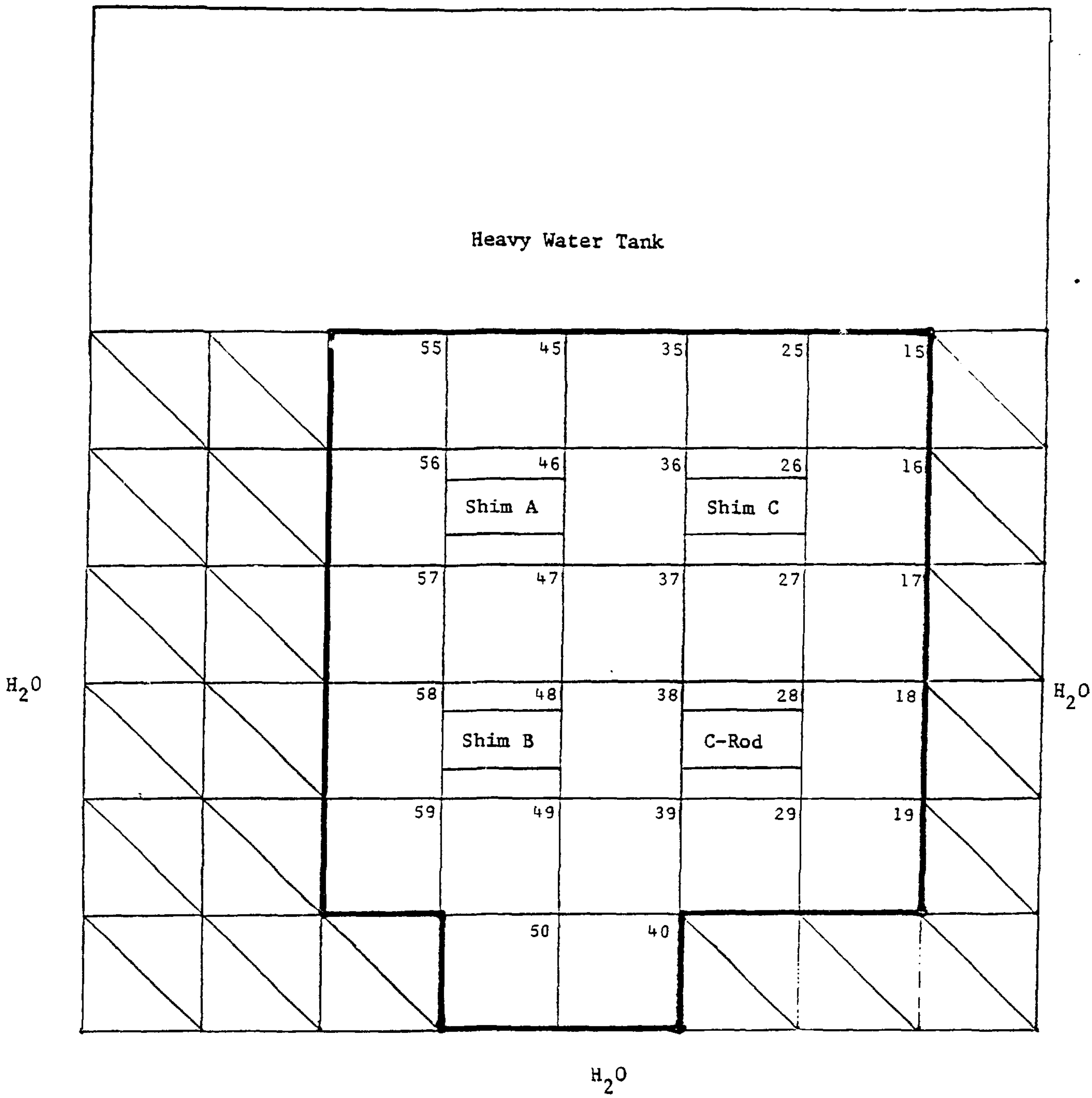

Fig. 2a FNR 27-Element LEU Core for Shim-Safety Rod Worth Measurements

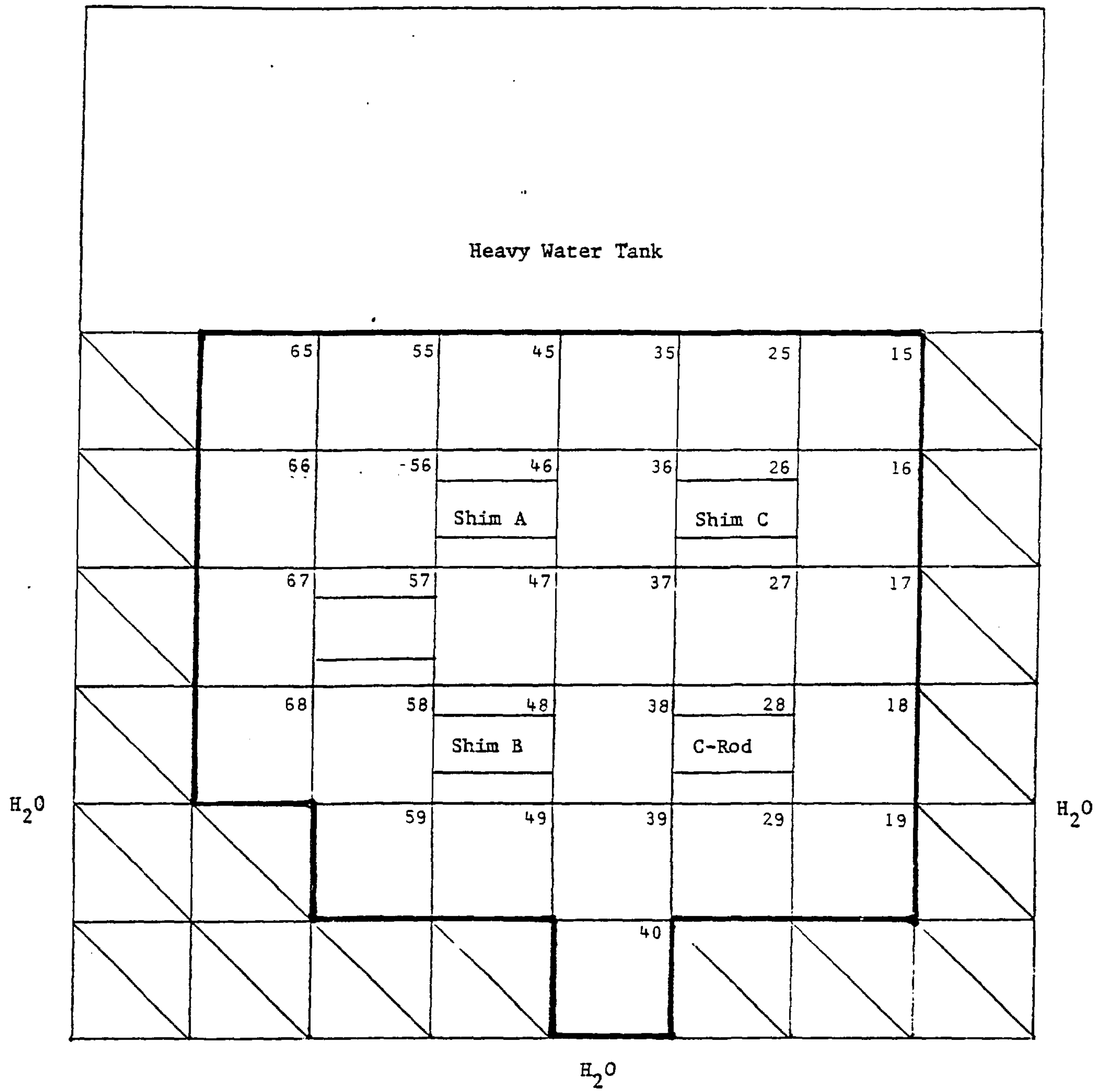

Fig. 2b FNR 30-Element LEU Core for Shim-Safety Rod Worth Measurements

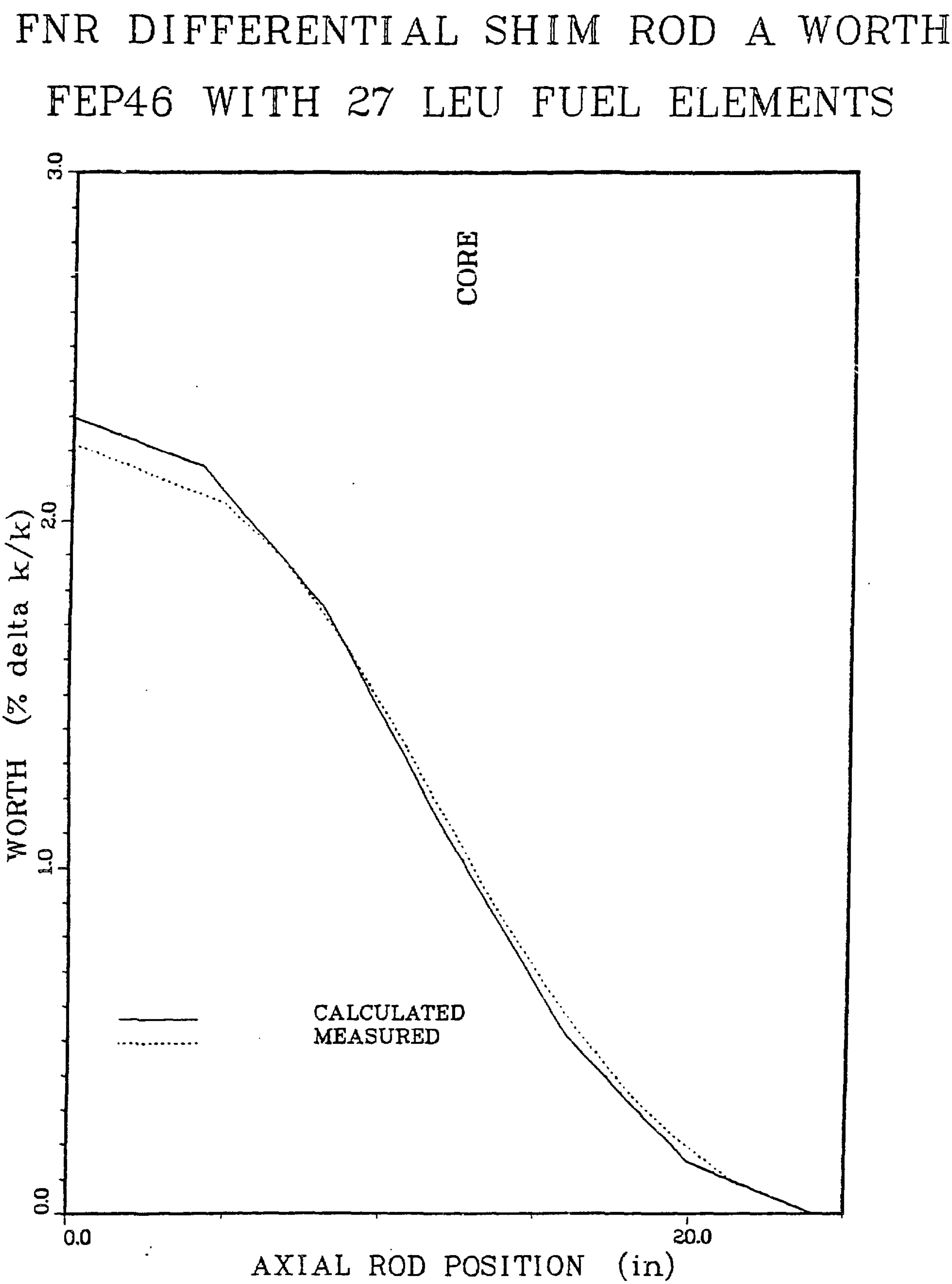
FNR DIFFERENTIAL SHIM ROD A WORTH
FEP46 WITH 27 LEU FUEL ELEMENTS
CORE
WORTH (% delta k/k)
3.0
2.0
1.0
0.0
0.0
20.0
AXIAL ROD POSITION (in)
CALCULATED
MEASURED

Fig. 3

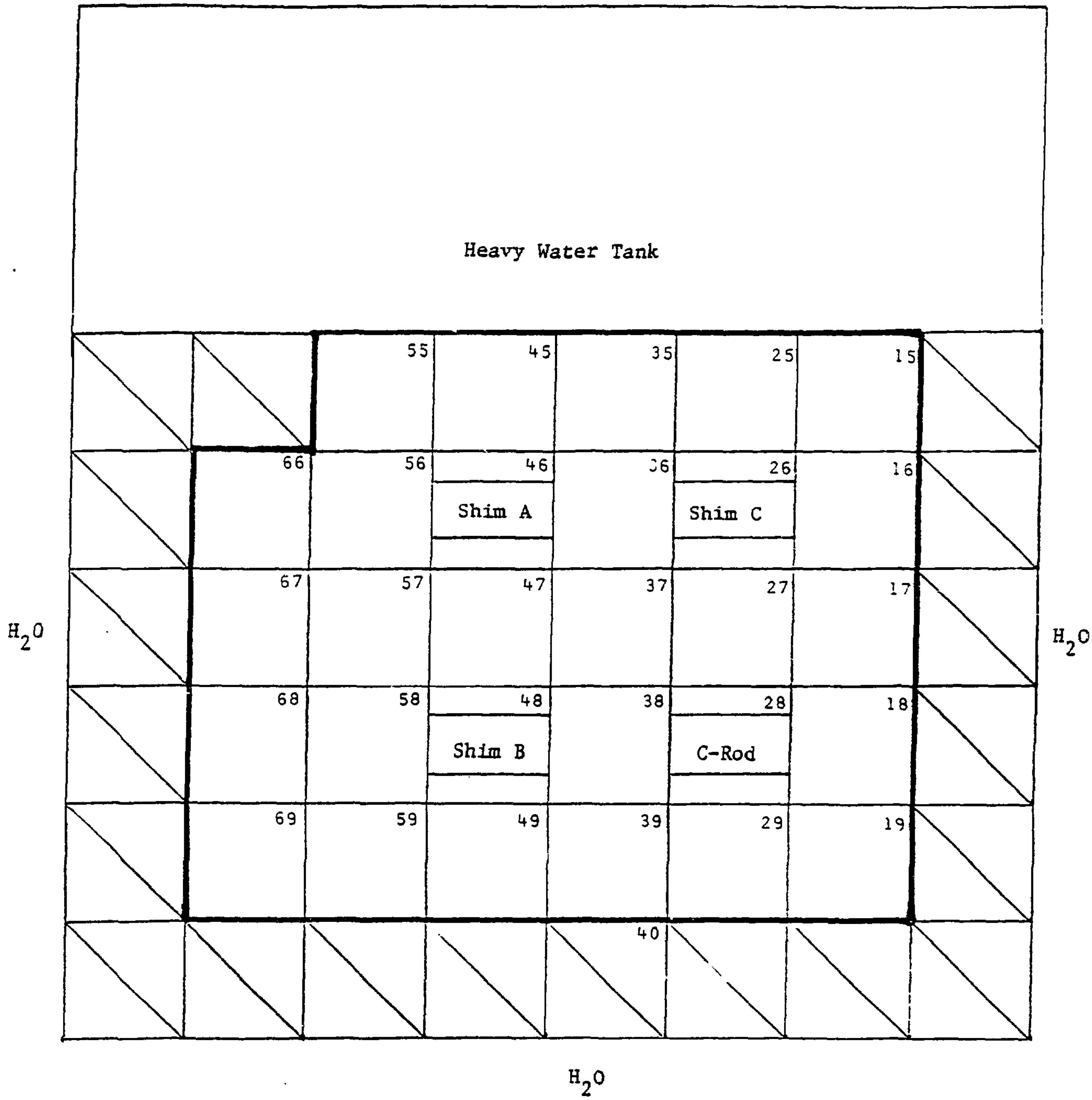

Fig. 4 FNR 29-Element LEU Core for Rhodium Reaction Rate Axial Distribution Measurements

RH AXIAL CAPTURE RATE DISTRIBUTIONS
FEP15 IN FNR WITH 29 LEU FUEL ELEMENTS

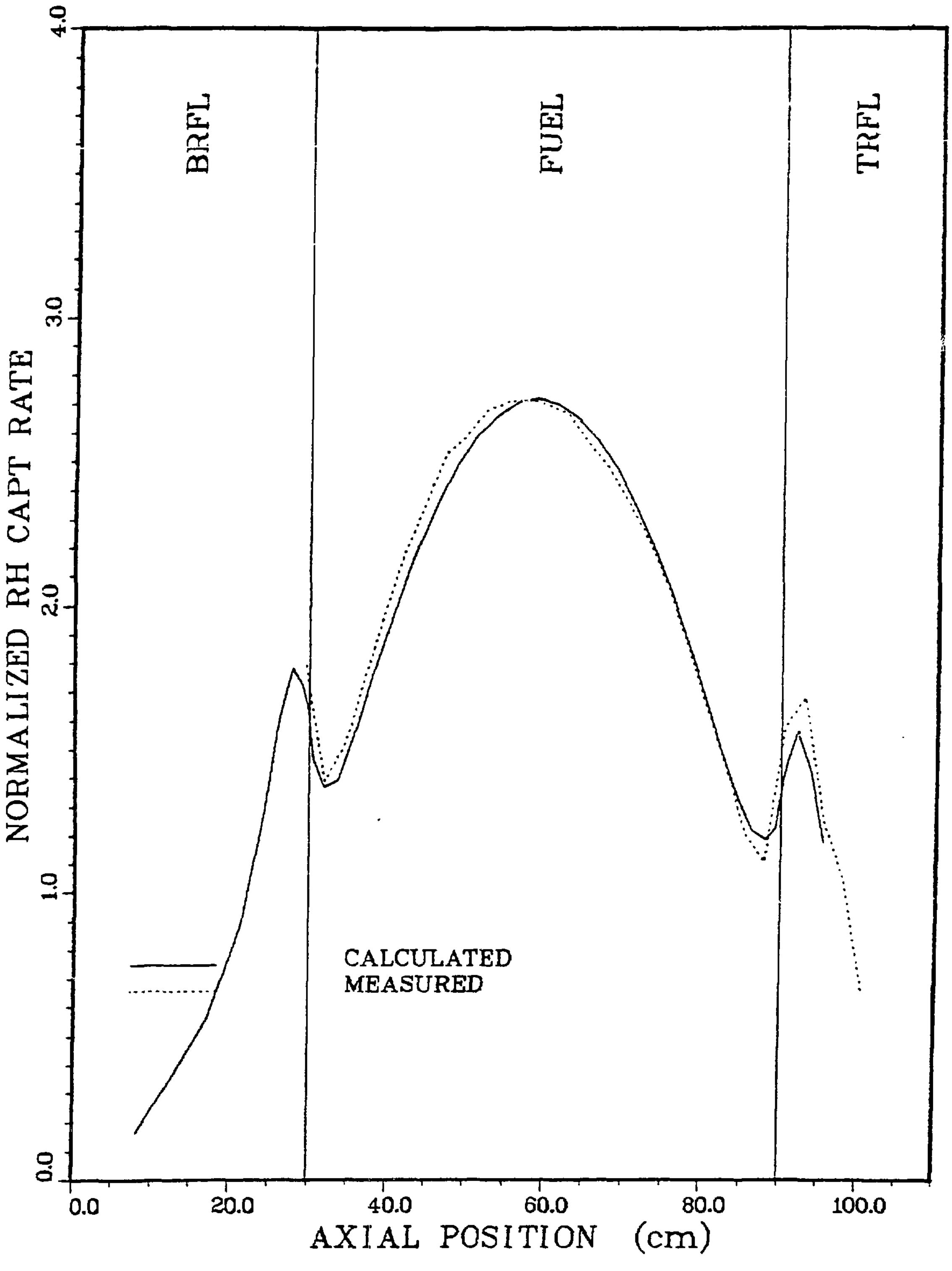

Fig. 5

RH AXIAL CAPTURE RATE DISTRIBUTIONS
FEP19 IN FNR WITH 29 LEU FUEL ELEMENTS

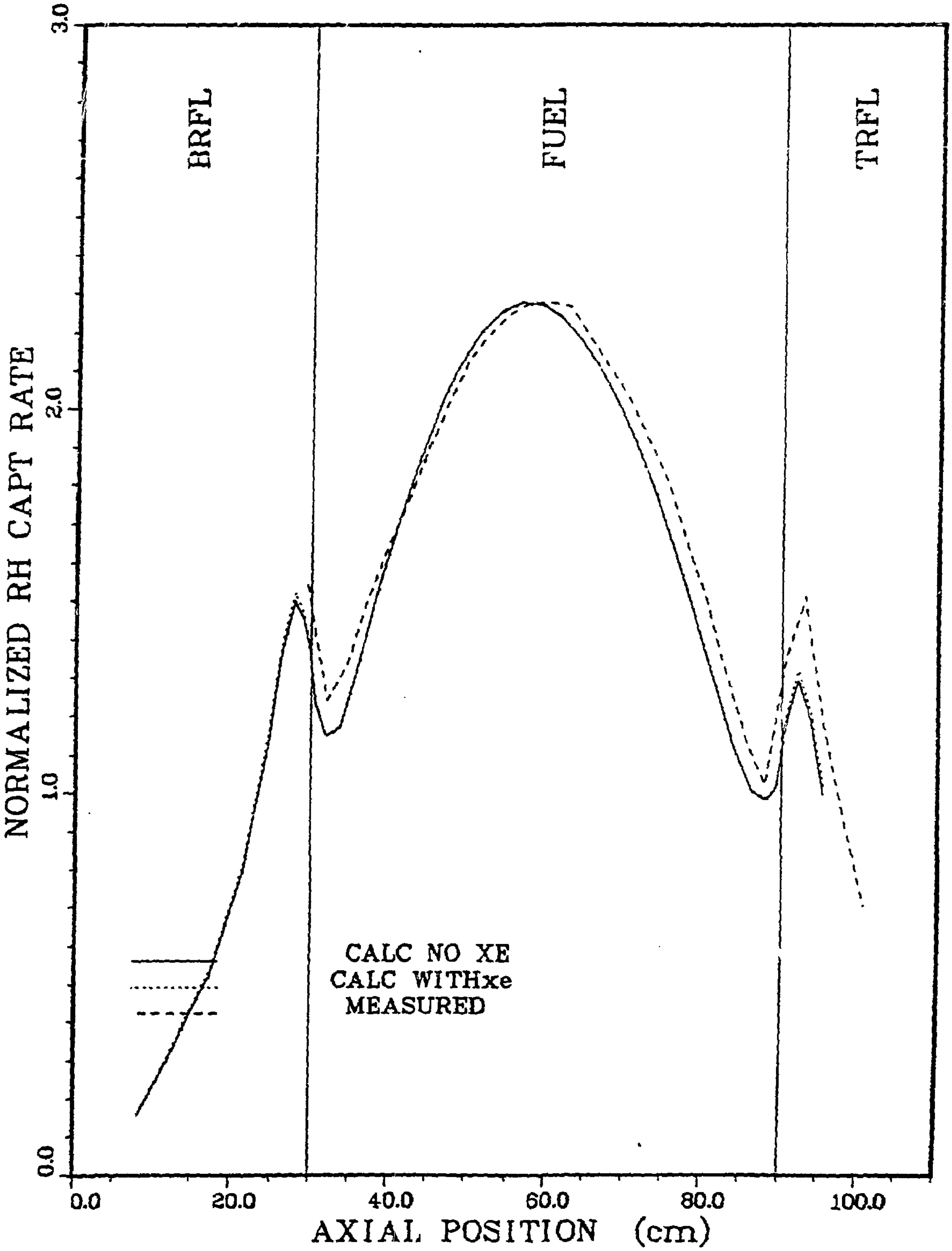

Fig. 6

RH AXIAL CAPTURE RATE DISTRIBUTIONS
FEP27 IN FNR WITH 29 LEU FUEL ELEMENTS

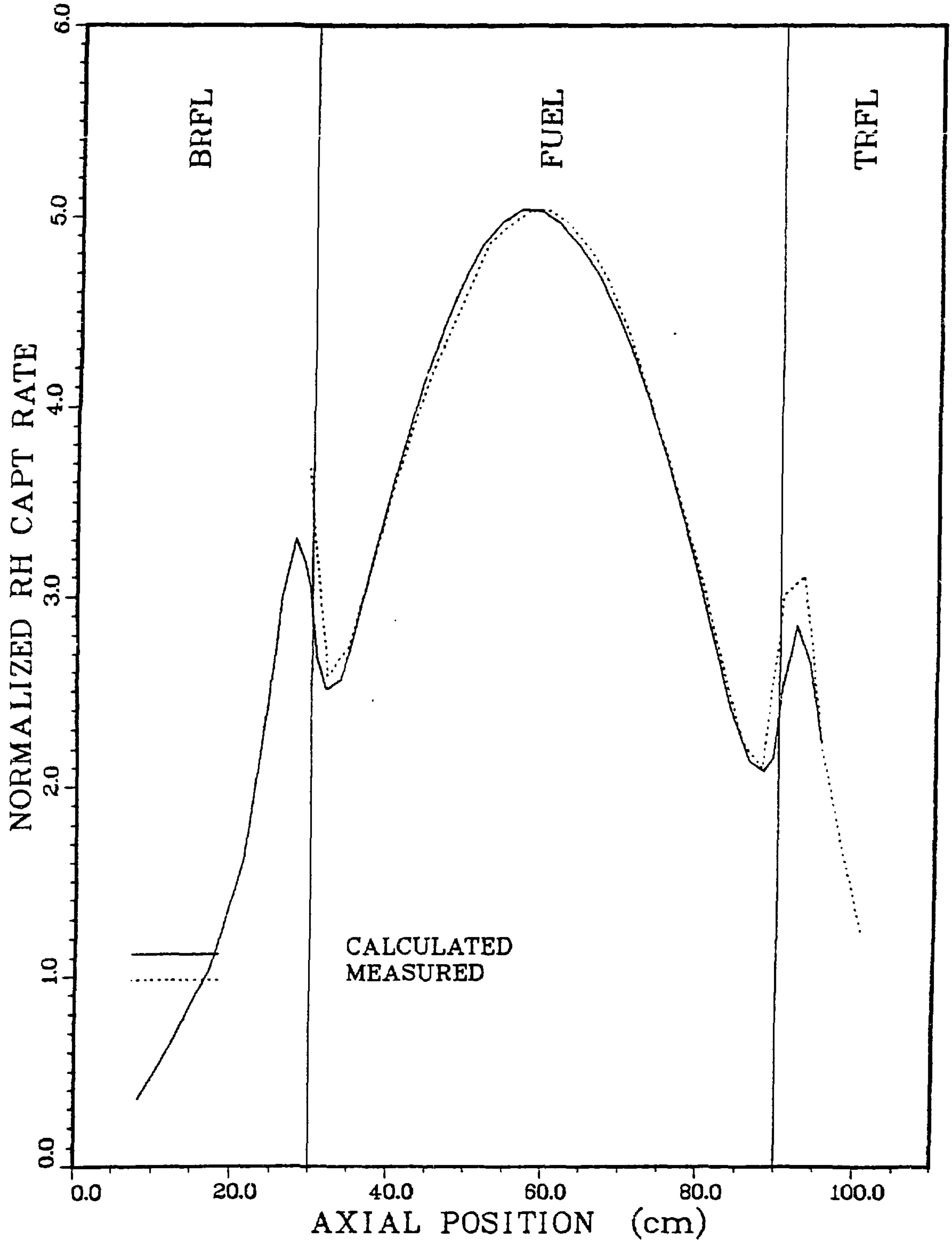

Fig. 7

RH AXIAL CAPTURE RATE DISTRIBUTIONS
FEP35 IN FNR WITH 29 LEU FUEL ELEMENTS

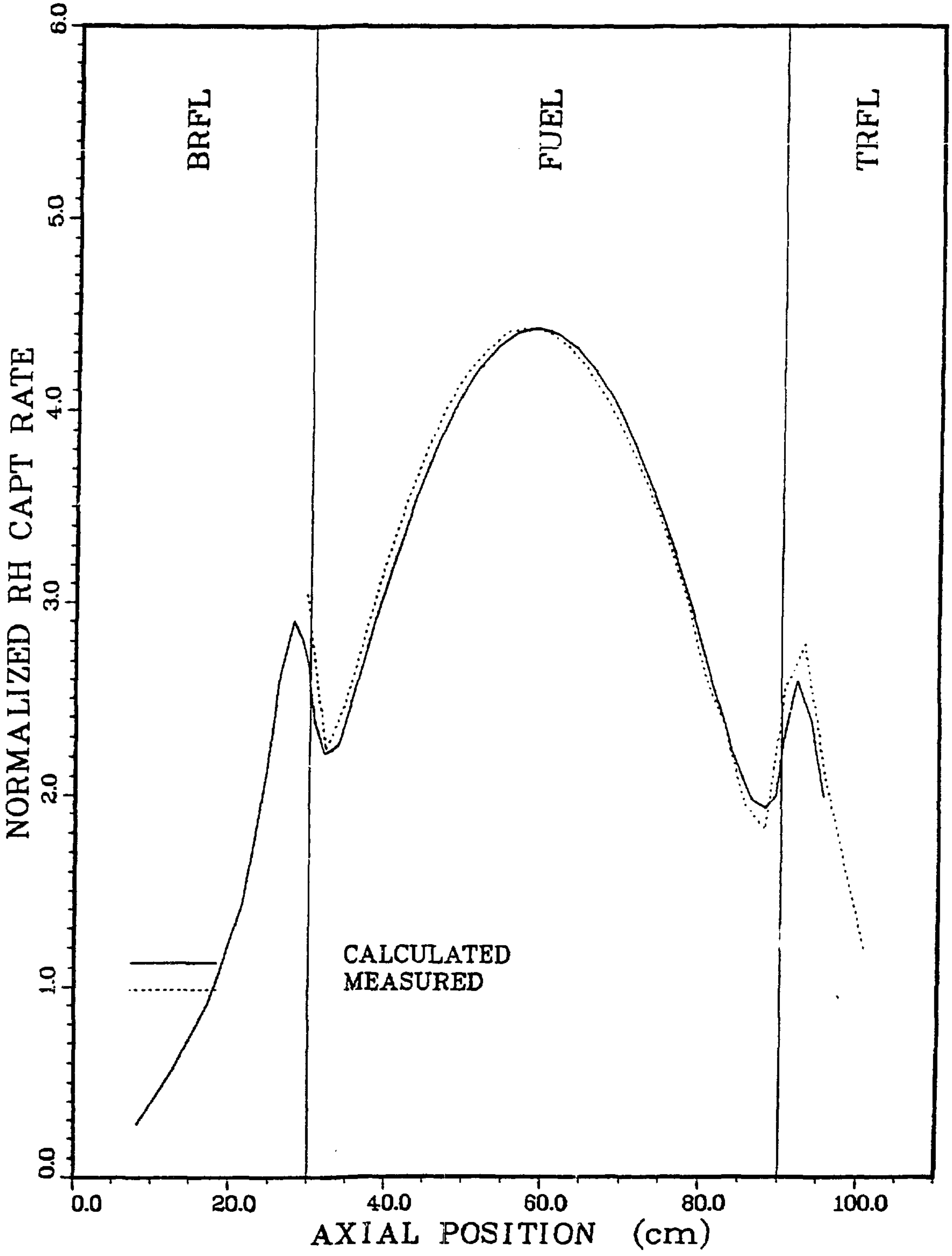

Fig. 8

RH AXIAL CAPTURE RATE DISTRIBUTIONS
FEP39 IN FNR WITH 29 LEU FUEL ELEMENTS

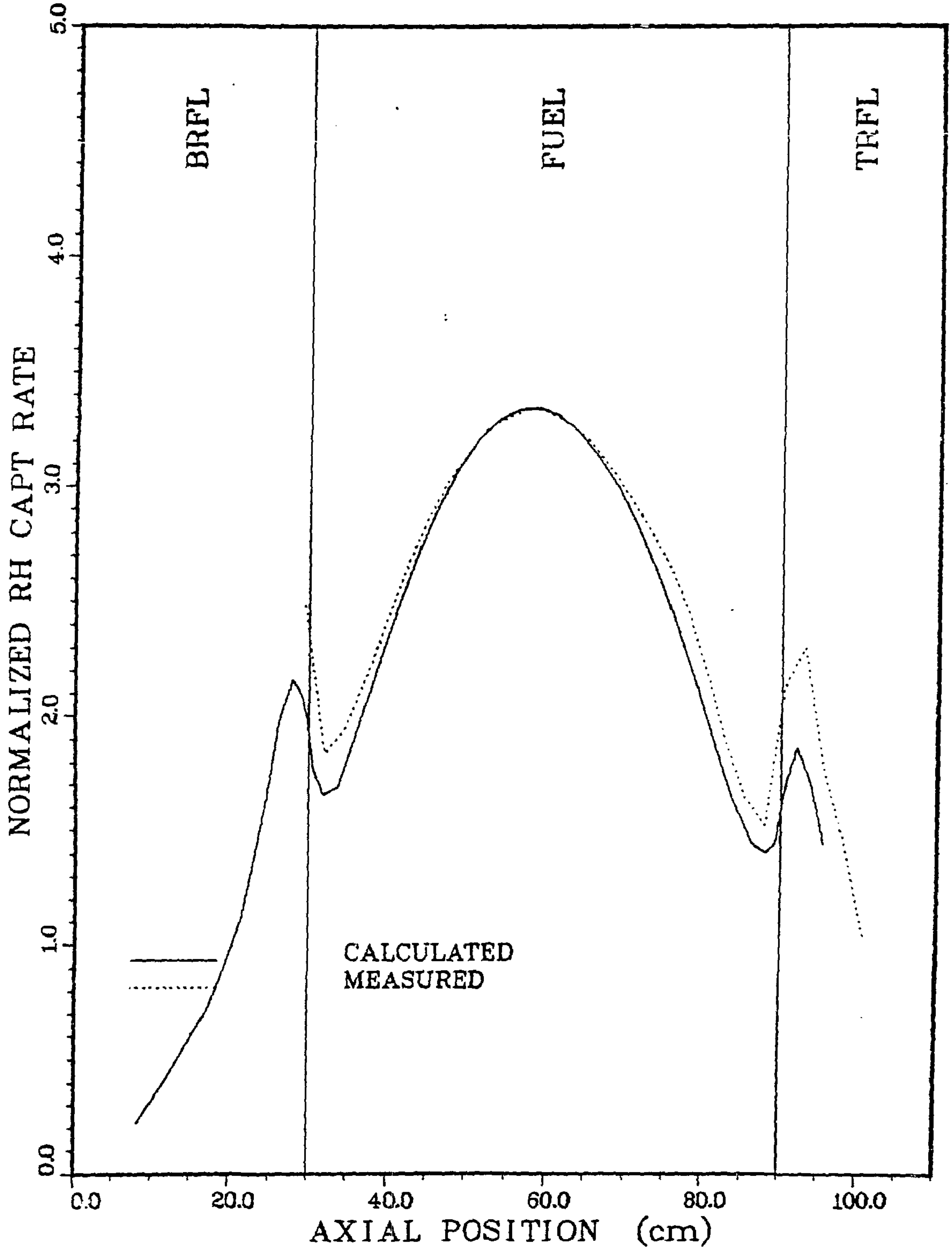

Fig. 9

RH AXIAL CAPTURE RATE DISTRIBUTIONS
FEP47 IN FNR WITH 29 LEU FUEL ELEMENTS

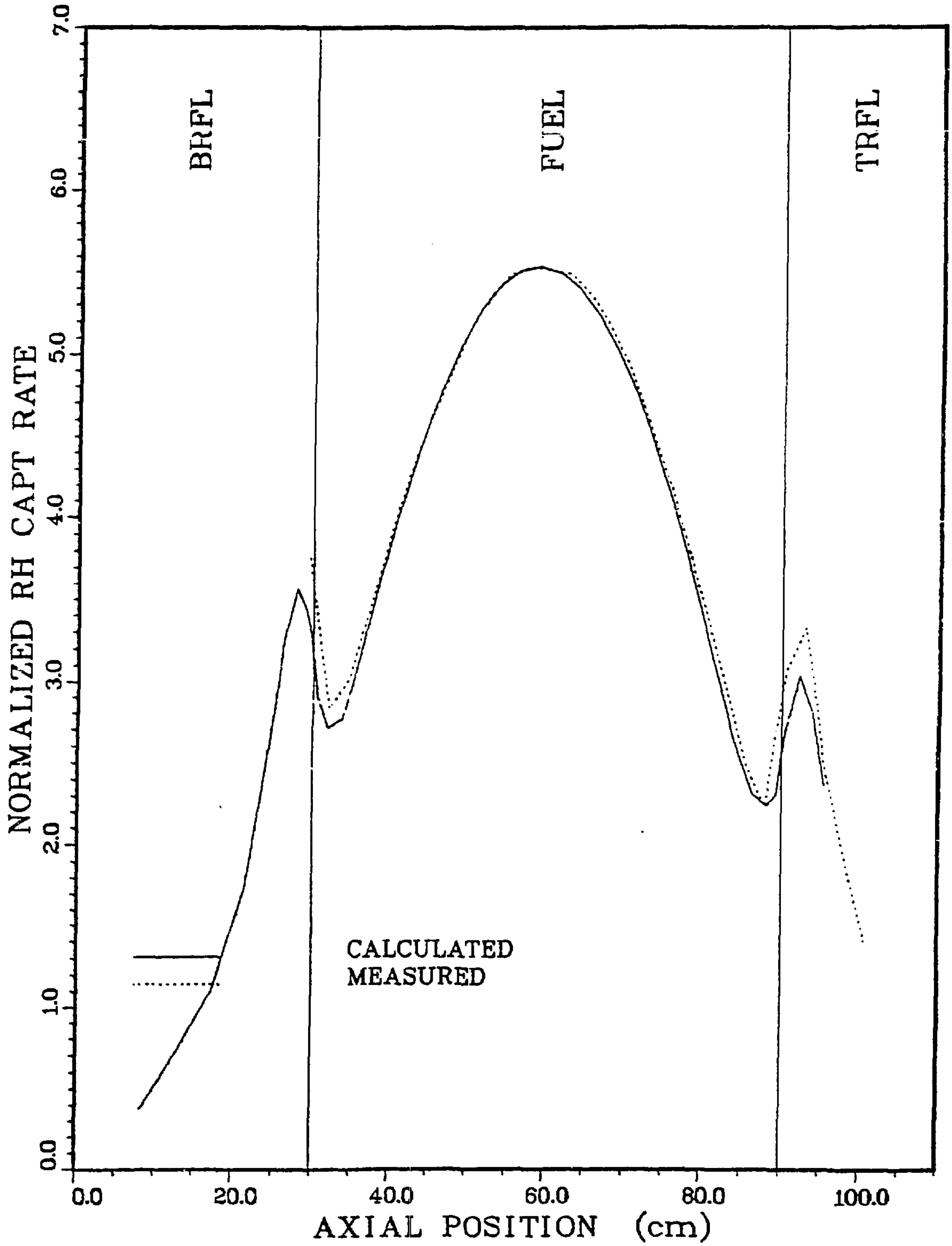

Fig. 10

RH AXIAL CAPTURE RATE DISTRIBUTIONS
FEP37 IN FNR WITH 29 LEU FUEL ELEMENTS

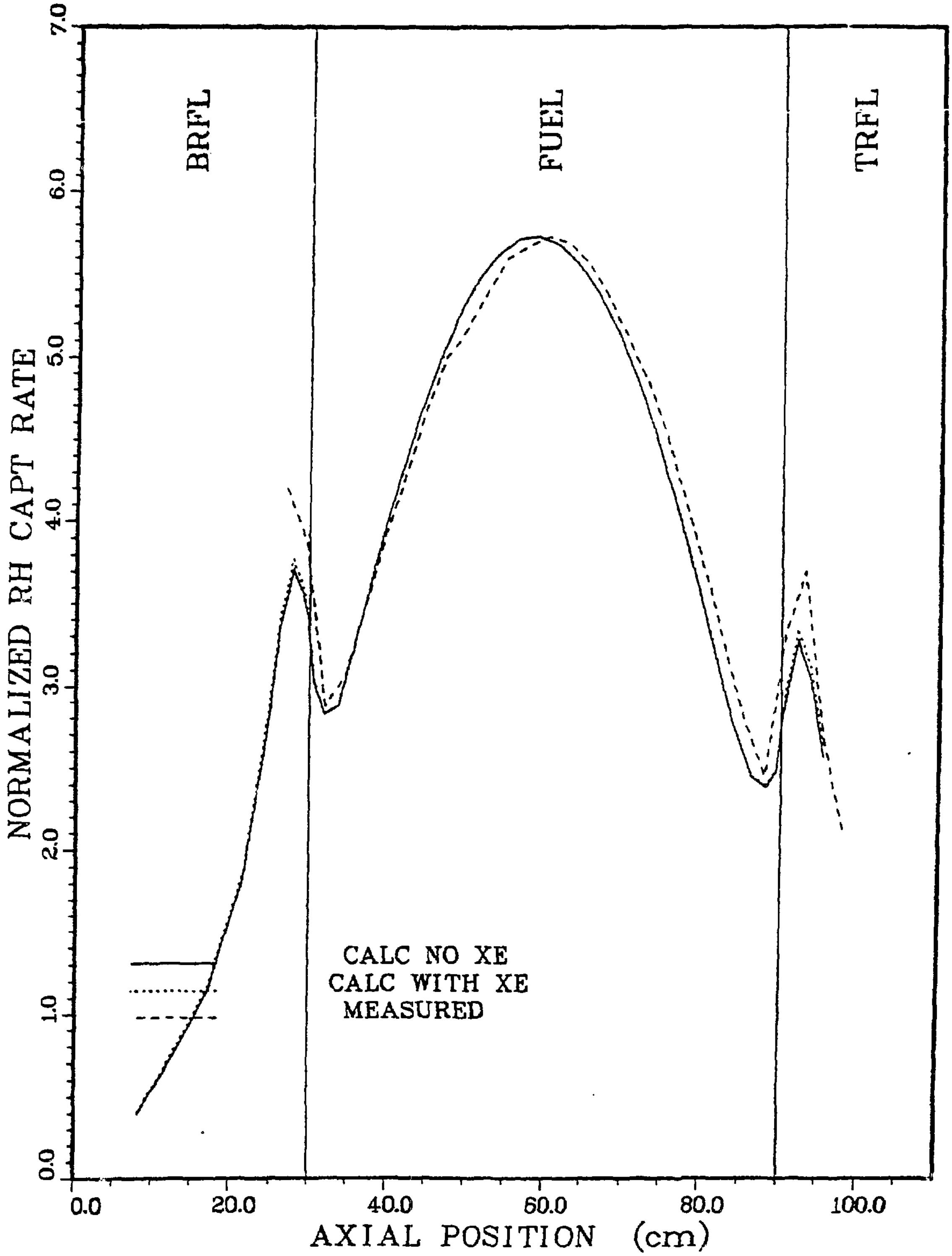

Fig. 11

RH AXIAL CAPTURE RATE DISTRIBUTIONS
FEP37 IN FNR WITH 29 LEU FUEL ELEMENTS

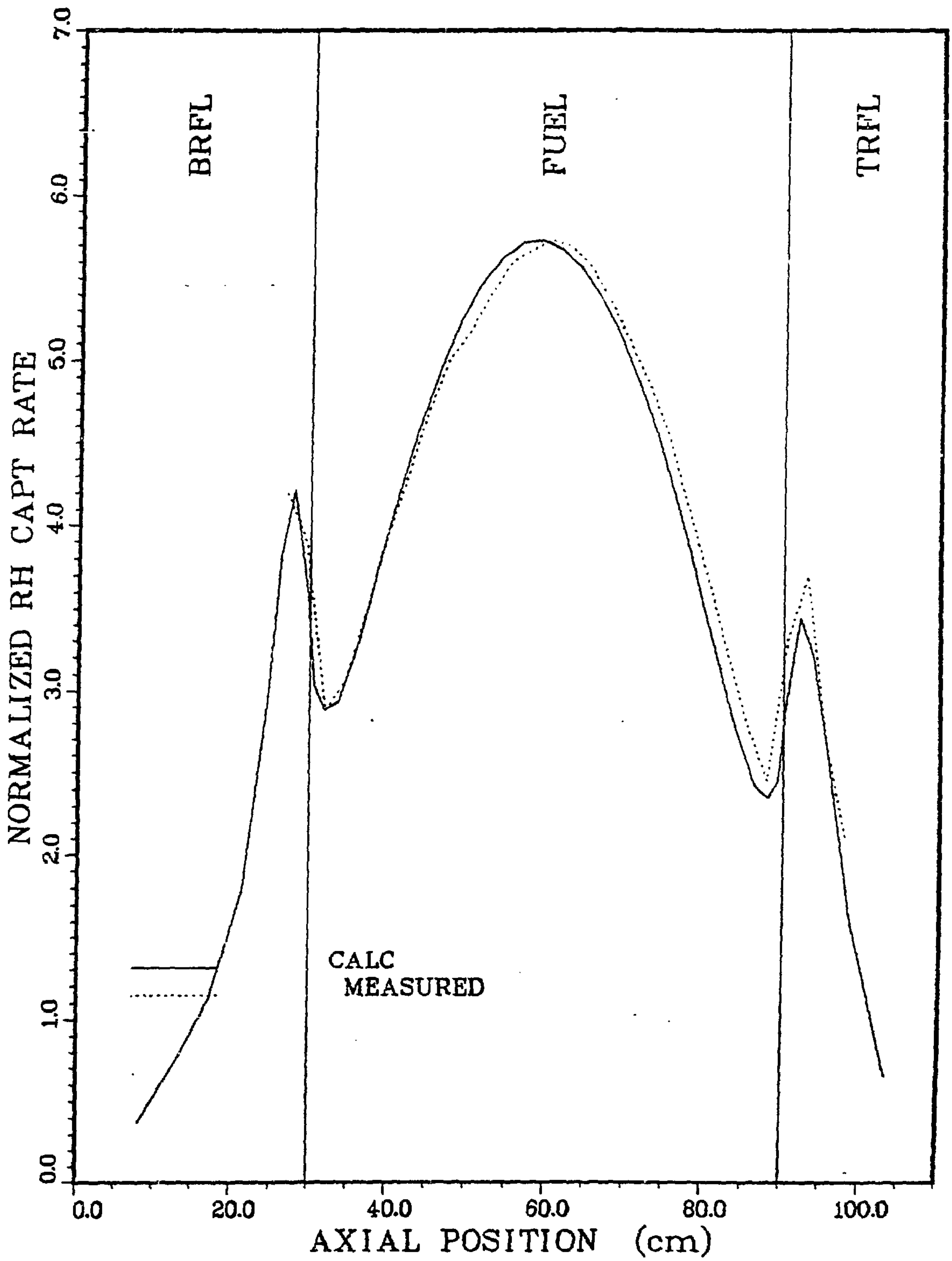

Fig. 12

RH AXIAL CAPTURE RATE DISTRIBUTIONS
H2OP40-3 FNR WITH 29 LEU FUEL ELEMENTS

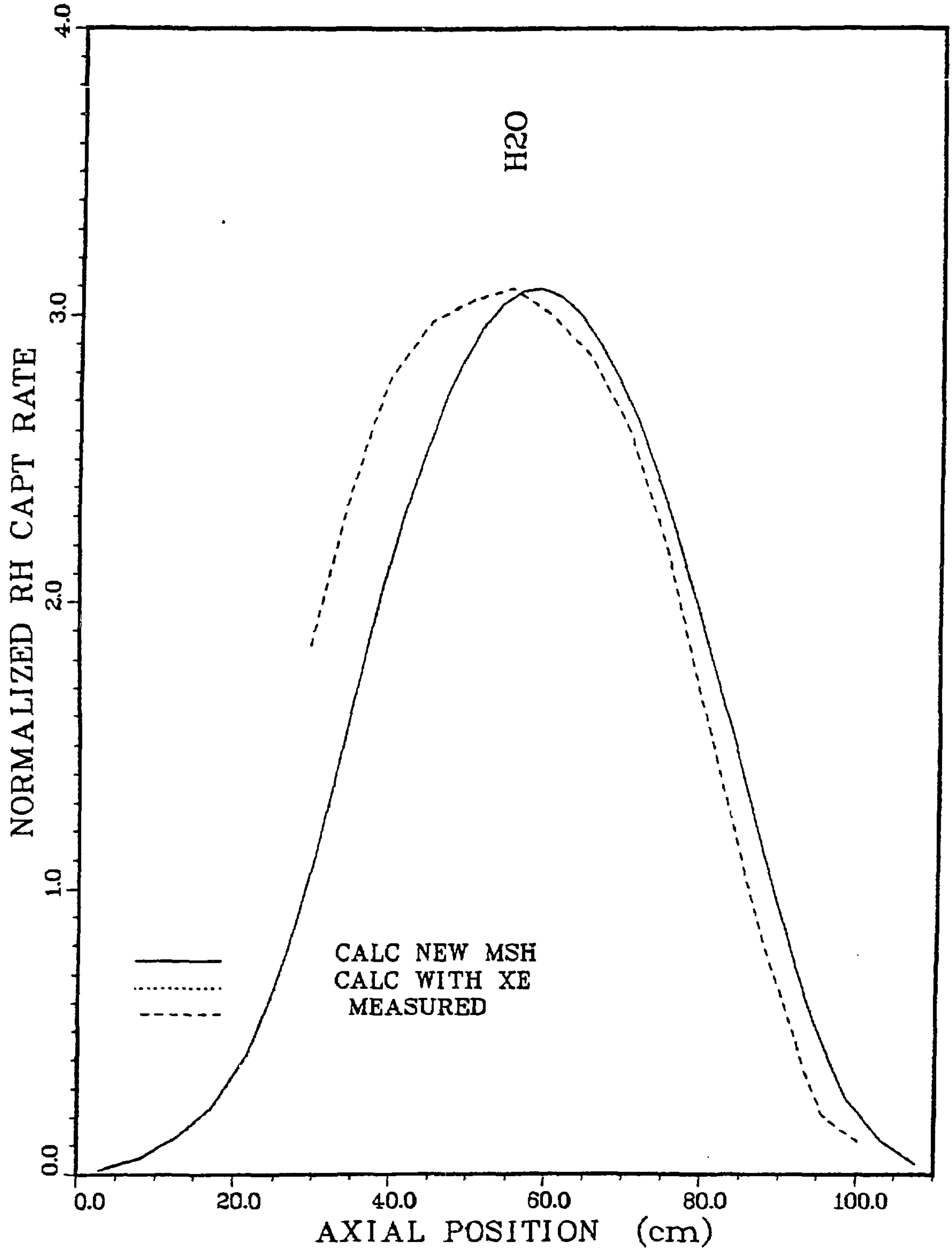

Fig. 13

Core side

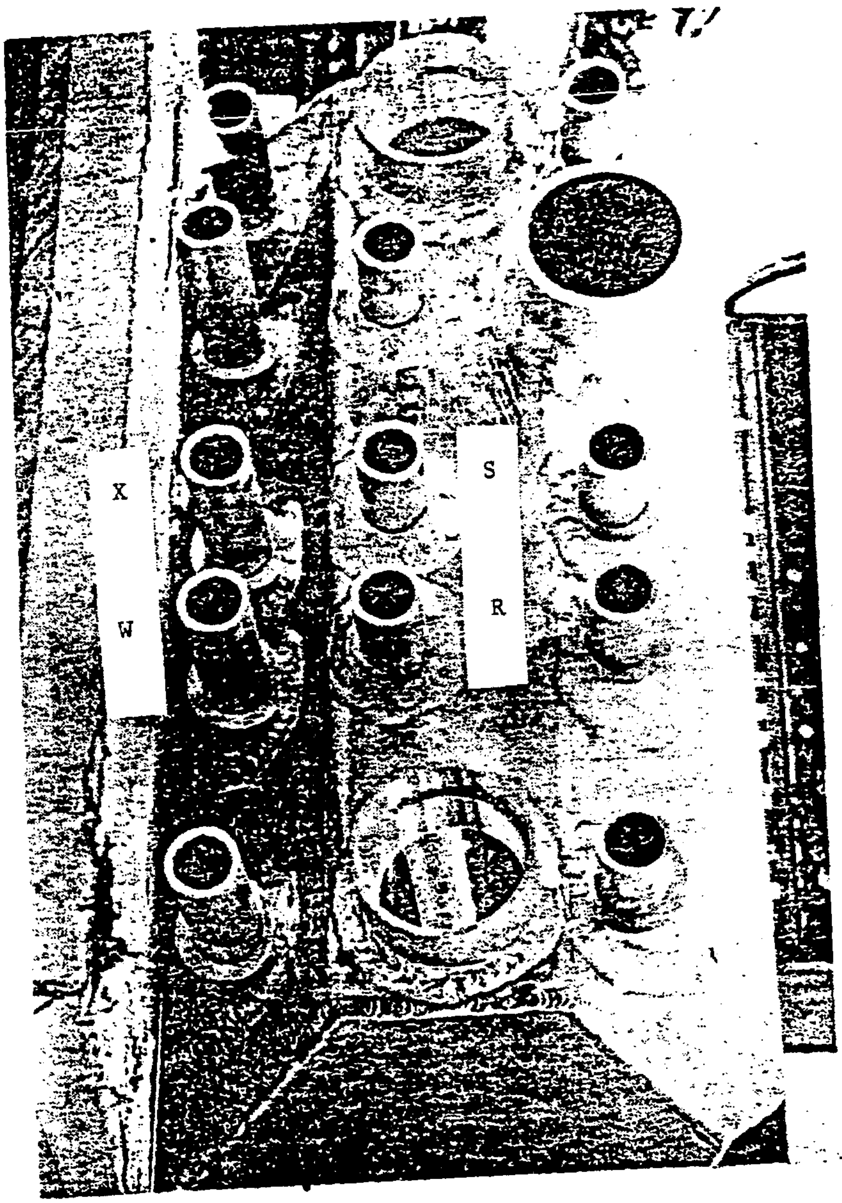

View of D_2O Tank Top from Above

Fig. 14

RH AXIAL CAPTURE RATE DISTRIBUTION
POSITION X IN D2O REFLECTOR TANK

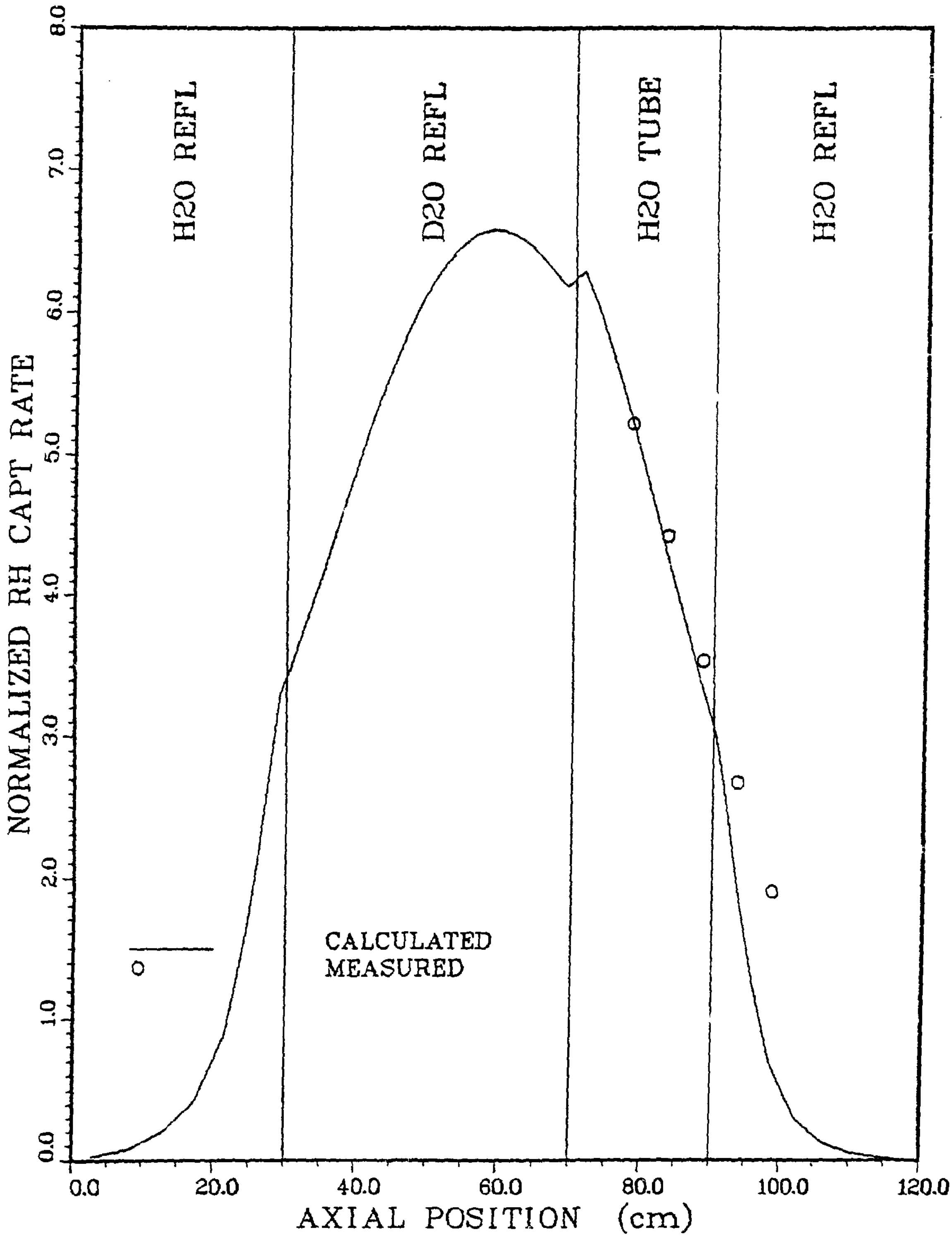

Fig. 15

RH AXIAL CAPTURE RATE DISTRIBUTION
POSITION S IN D2O REFLECTOR TANK

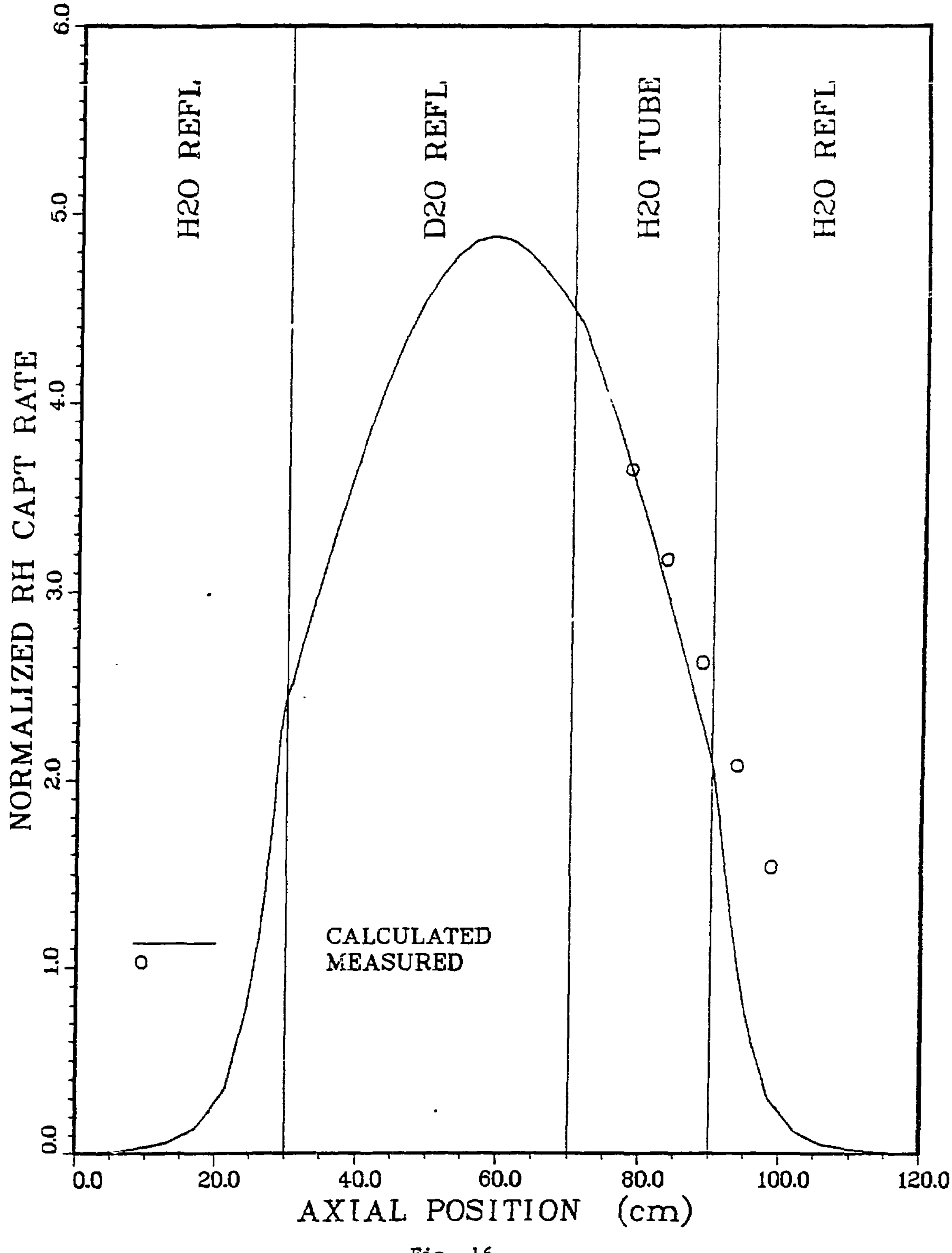

Fig. 16

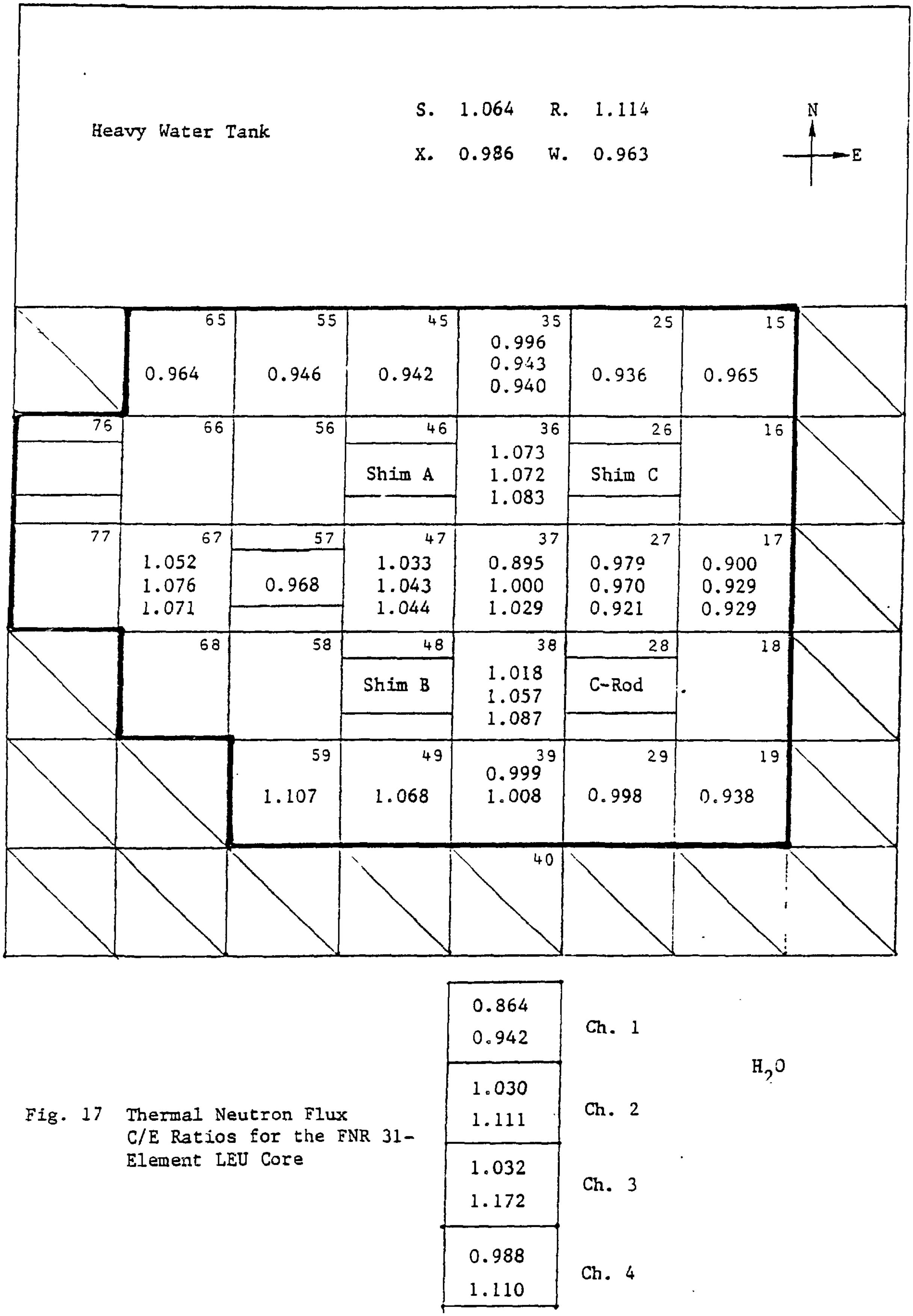

Fig. 17 Thermal Neutron Flux C/E Ratios for the FNR 31-Element LEU Core

THERMAL FLUX DISTRIBUTION IN ROW 7 OF THE FNR WITH 31 LEU FUEL ELEMENTS

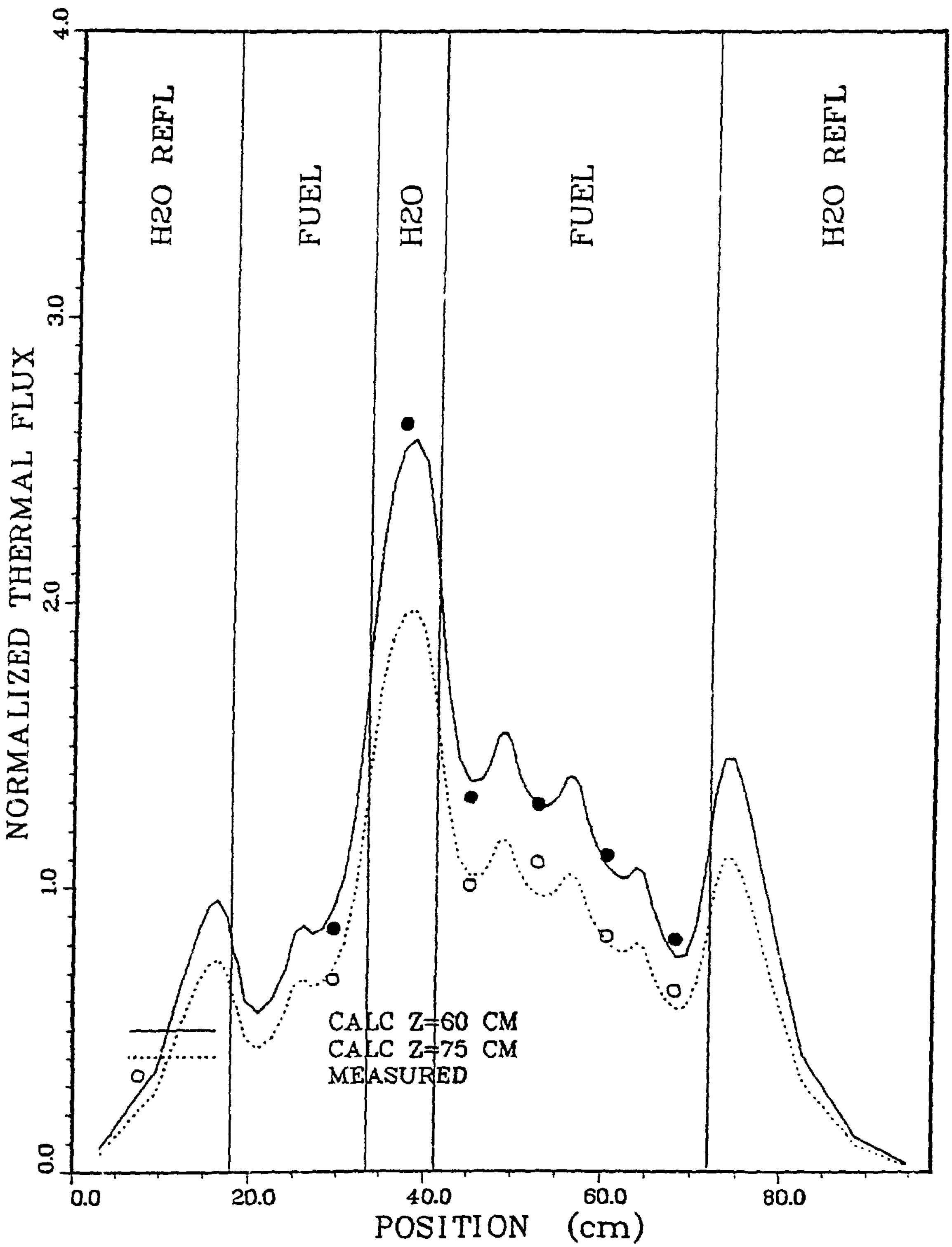

Fig. 18

THERMAL FLUX DISTRIBUTION IN COLUMN 3
OF THE FNR THRU D2O POSITIONS W AND R

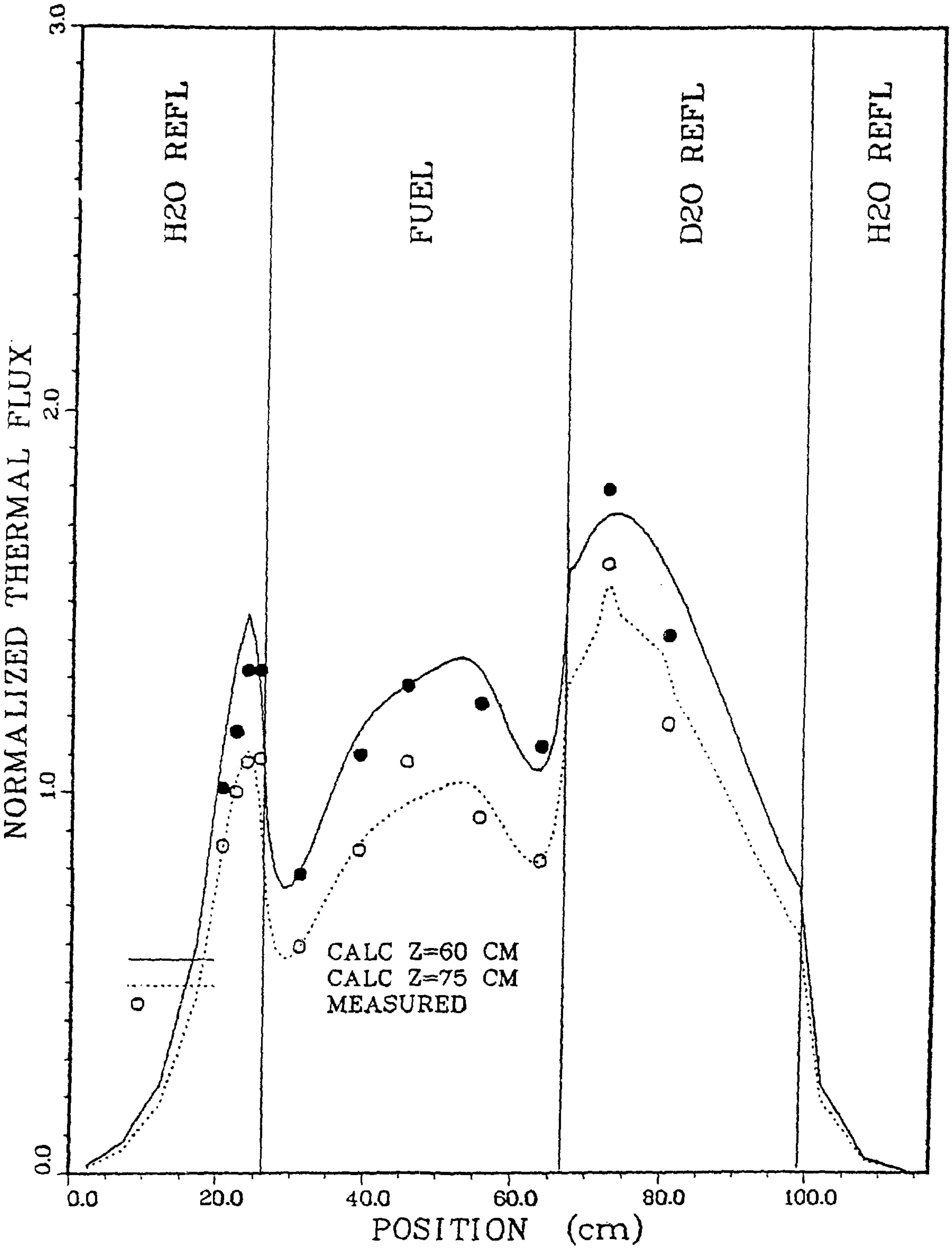

Fig. 20

THERMAL FLUX DISTRIBUTION IN COLUMN 3
OF THE FNR THRU D2O POSITIONS X AND S

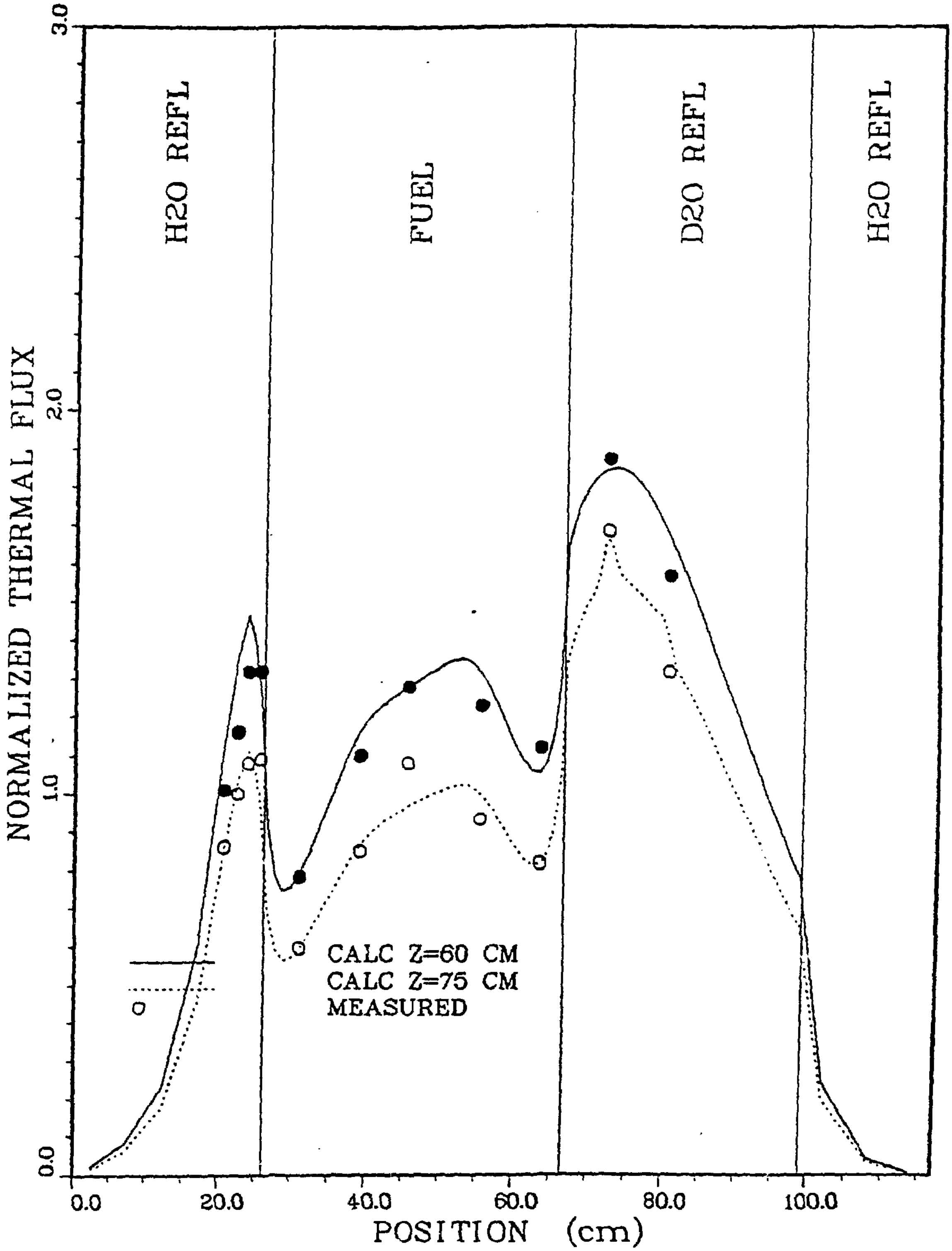

Fig. 19